






Coexistence of random singlets and disordered Kitaev spin liquid in $\text{H}_3\text{LiIr}_2\text{O}_6$

Chanhyeon Lee ^{1,*}, Suheon Lee,^{2,*} Youngsu Choi,^{3,*} C. Wang,⁴ H. Luetkens,⁴ T. Shiroka ⁴, Zeehoon Jang ⁵,
Young-Gui Yoon ^{1,†} and Kwang-Yong Choi ^{6,‡}

¹*Department of Physics, Chung-Ang University, Seoul 06974, Republic of Korea*

²*Center for Integrated Nanostructure Physics, Institute for Basic Science (IBS), Suwon 16419, Republic of Korea*

³*Department of Energy Science, Sungkyunkwan University, Suwon 16419, Republic of Korea*

⁴*Laboratory for Muon Spin Spectroscopy, Paul Scherrer Institute, 5232 Villigen, Switzerland*

⁵*Department of Physics, Kookmin University, Seoul 02707, Republic of Korea*

⁶*Department of Physics, Sungkyunkwan University, Suwon 16419, Republic of Korea*



(Received 21 August 2022; revised 1 January 2023; accepted 17 January 2023; published 30 January 2023)

We combine static magnetic susceptibility $\chi(T)$, muon-spin relaxation, and ^1H nuclear magnetic resonance measurements to explore the spin dynamics in the disordered-induced quantum spin liquid candidate $\text{H}_3\text{LiIr}_2\text{O}_6$. Inverse Laplace transform analysis of the ^1H spin-lattice relaxation rate $1/T_1$ enables us to identify two characteristic temperatures $T_g = 110\text{ K}$ and $T^* = 26\text{ K}$. Below T_g , a slower $1/T_1^{\text{slow}}$ component dictated by gapped excitations with a spin gap $\Delta_h = 30\text{--}38\text{ K}$ evolves distinctly from a faster $1/T_1^{\text{fast}}$ component pertaining to gapless excitations. Furthermore, we observe a sub-Curie divergent $\chi(T) \propto T^{-0.68}$, a power-law dependent $1/T_1^{\text{fast}} \propto T^{1.4}$, and a weakly activated $1/T_1^{\text{slow}} \propto \exp(-\Delta_l/k_B T)$ ($\Delta_l = 3\text{--}6\text{ K}$) below $T^* = 26\text{ K}$. All these features suggest the coexistence of a disordered spin-liquid state and spin singlets with spatially distributed gaps.

DOI: [10.1103/PhysRevB.107.014424](https://doi.org/10.1103/PhysRevB.107.014424)

I. INTRODUCTION

Kitaev's exactly solvable model on a honeycomb lattice has marked a significant step in the quest for quantum spin liquids (QSLs). The elementary excitations of Kitaev QSLs comprise itinerant Majorana fermions coupled to a static Z_2 gauge at zero field [1]. Inspired by Jackeli and Khaliullin's proposal [2], intensive research has been conducted on $j_{\text{eff}} = 1/2$ spin-orbit assisted Mott insulators as potential candidates for materializing Kitaev magnetism, including honeycomb iridates A_2IrO_3 ($\text{A} = \text{Na}, \text{Li}$) and ruthenate $\alpha\text{-RuCl}_3$ [3–8]. Despite the dominant Kitaev interactions, no reported materials are known to achieve a genuine Kitaev QSL due to the inevitable presence of non-Kitaev terms.

On the other side, certain types of quenched disorders in QSL candidates are suggested to expedite a quantum disordered or random-singlet state against long-range magnetic order [9–16]. The conspicuous effects of the disorder have been showcased in the H-intercalated iridate $\text{H}_3\text{LiIr}_2\text{O}_6$ [17,18]. Previous thermodynamic, nuclear magnetic resonance (NMR), and muon spin relaxation (μSR) measurements negated a magnetic transition down to 50 mK [18,19]. Singularly, a dome-shaped magnetic continuum observed by Raman spectroscopy alludes to fractionalized spin excitations [20]. Furthermore, the divergent specific heat $C/T \sim T^{-0.5}$ and the time-field scaling of the μSR spectra $A(t) \sim A(t/H)^{0.46}$

are taken as evidence for the abundant low-energy density of states (DOS) $N(E) \sim E^{-0.5}$ generated by disorders [19,21,22].

Initially, $\text{H}_3\text{LiIr}_2\text{O}_6$ was thought to be a spin-orbital-entangled QSL. However, subsequent theoretical and experimental studies identified several forms of quenched disorders: static or dynamic disorder of the interlayer hydrogen, stacking faults, and nonmagnetic Ir^{3+} ($3d^6$) defects [21,23–27]. Static or dynamic hydrogen disorders lead to a quantum-disordered paraelectric and a QSL-like state with enhanced Kitaev exchange or with random Kitaev-like bonds [27–29]. Conversely, defect-induced disorder can provide a route to the observed QSL state without resorting to the renormalization of Kitaev exchange [20]. Actually, the power-law distribution of the low-energy DOS is equally well captured by the Kitaev model subject to bond disorder or spin vacancies [21,22,30]. It is notable that the related Kitaev candidate materials Cu_2IrO_3 , $\text{Ag}_3\text{LiIr}_2\text{O}_6$, and $\alpha\text{-(Ru,Ir)Cl}_3$ display commonly disordered QSLs that feature spatially inhomogeneous local excitations and ground states [31–36].

As such, it is imperative to clarify whether a putative inhomogeneous ground state of $\text{H}_3\text{LiIr}_2\text{O}_6$ comprises heterogeneous magnetic states as reported in other disordered Kitaev materials. However, disentangling the impact of bond disorder and nonmagnetic defects on a ground state and spin dynamics is experimentally challenging. In this situation, NMR is capable of disentangling various inhomogeneous ground states, insofar as full information about spin dynamics is attained from an unbiased analysis of the nuclear magnetization curve $M(t)$ using the inverse Laplace transform (ILT) method [15,36,37].

*These authors contributed equally to this work.

†Corresponding author: yyoon@cau.ac.kr

‡Corresponding author: choisky99@skku.edu

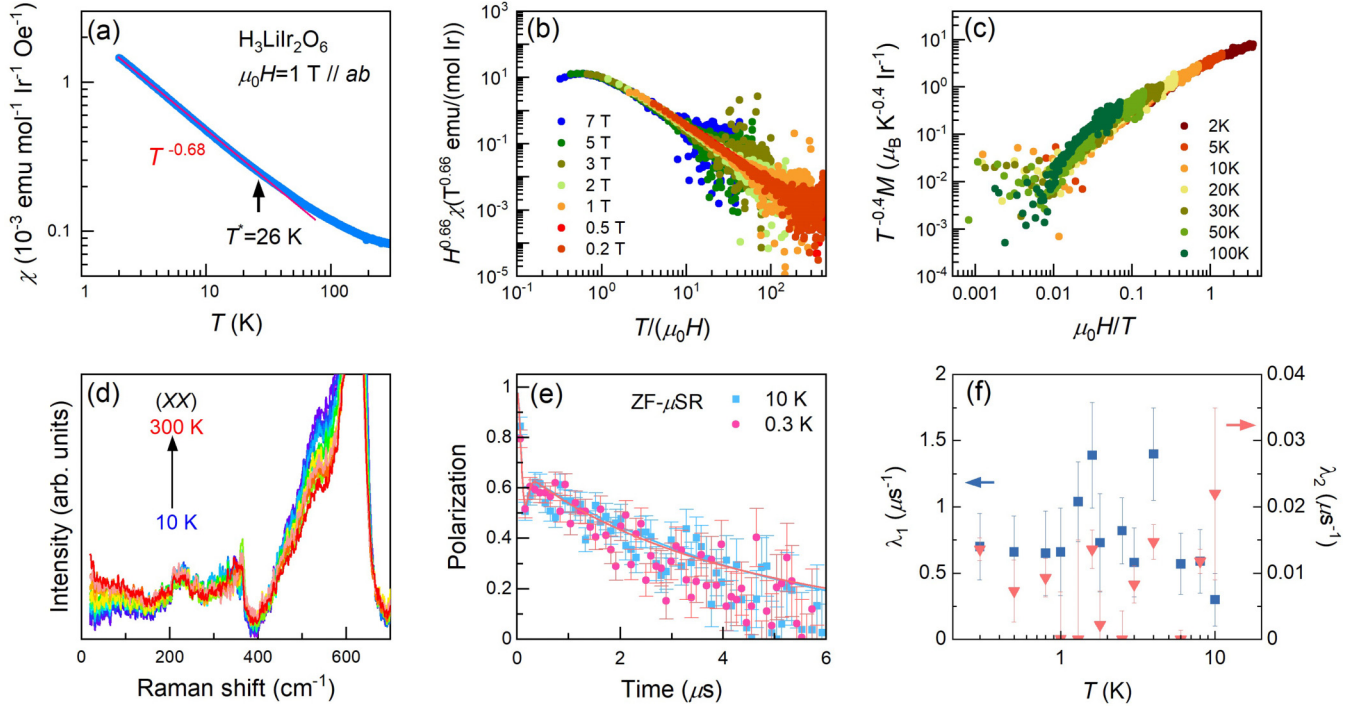


FIG. 1. (a) Log-log plot of the static magnetic susceptibility $\chi(T)$ versus temperature measured at $\mu_0 H = 1 \text{ T} \parallel ab$. The solid line denotes a sub-Curie increase $T^{-0.68}$ below $T^* = 26 \text{ K}$ (vertical arrow). (b) Scaling of $H^{0.66}\chi(T)$ with T/H . (c) Log-log scaled plot of $T^{-0.4}M(H)$ versus H/T . (d) Thermal evolution of the Raman spectra in parallel polarization. (e) Representative muon spin polarization at zero field with the fitted curves as described in the main text. (f) Temperature dependence of the two muon spin relaxation rates $\lambda_1(T)$ and $\lambda_2(T)$.

In this paper, we illuminate the nature of an inhomogeneous ground state in $\text{H}_3\text{LiIr}_2\text{O}_6$ by deducing the density distribution function $P(1/T_1)$ of the ^1H NMR spin-lattice relaxation rate $1/T_1$ using the ILT technique. On cooling through two characteristic temperatures $T_g = 110 \text{ K}$ and $T^* = 26 \text{ K}$, we uncover the distinct evolution of a disordered QSL state and spin singlets with spatially distributed gaps, demonstrating the multifaceted impact of disorder on Kitaev materials.

II. EXPERIMENTAL DETAILS

Single crystals of $\text{H}_3\text{LiIr}_2\text{O}_6$ were prepared by a standard hydrothermal reaction with seed single-crystal $\alpha\text{-Li}_2\text{IrO}_3$ sample [38]. The grown crystals were characterized by x-ray powder diffraction using $\text{Cu } K\alpha$ radiation (the D8-advanced model) and Raman scattering measurements (see Appendix A).

Raman spectra were measured in backscattering geometry with a micro-Raman spectrometer (XperRama200VN, Nanobase) equipped with an air-cooled charge-coupled device (Andor iVac Camera) and the excitation line $\lambda = 532 \text{ nm}$ of DPSS SLM laser. We employed a notch filter to reject Rayleigh scattering down to a lower cutoff frequency of 20 cm^{-1} . The laser beam with $P = 280 \mu\text{W}$ was focused on a few-micrometer-diameter spot on the surface of the crystals using a $\times 40$ magnification microscope objective. The samples were placed in a liquid-He-cooled continuous flow cryostat at temperatures between 4.3 and 300 K.

^1H ($I = 1/2$, $\gamma_N = 42.5774 \text{ MHz/T}$) NMR measurements were conducted using a MagRes spectrometer and a 14 T

Oxford Teslatron superconducting magnet. ^1H NMR spectra were acquired by a fast Fourier transform of spin-echo signals with $\pi/2$ pulse length $\tau_{\pi/2} = 1.2\text{--}2 \mu\text{s}$, while applying an external magnetic field along the honeycomb ab plane. The nuclear spin-lattice (spin-spin) relaxation time T_1 (T_2) was measured by the saturation recovery (Hahn echo) method.

Zero-field (ZF) and longitudinal-field (LF) μSR experiments were conducted on the Dolly spectrometer of the Paul Scherrer Institute (Villigen, Switzerland) using a ^3H cryostat ($0.3 < T < 10 \text{ K}$). The single crystals of $\text{H}_3\text{LiIr}_2\text{O}_6$ were finely ground and glued with ethanol-diluted GE varnish on a Cu plate. The detector efficiency α between forward and backward positron detectors was determined by applying a weak transverse field $H_{\text{TF}} = 30 \text{ G}$ at $T = 0.3$ and 10 K . We analyzed all the μSR data using the software package MUSRFIT [39].

III. RESULTS AND DISCUSSION

A. Magnetic susceptibility, magnetization, Raman spectra, and μSR

Given that a degree of quenched disorders (thereby magnetic parameters) is conditioned by the details of soft-chemical treatment, it is a due procedure to check the structural and magnetic properties of our samples. We first discuss the T dependence of the dc magnetic susceptibility $\chi(T)$ of $\text{H}_3\text{LiIr}_2\text{O}_6$ for $\mu_0 H \parallel ab$. As exhibited in Fig. 1(a), a log-log plot of $\chi(T)$ reveals a sub-Curie divergence $\chi(T) \propto T^{-0.68}$ for temperatures below $T^* = 26 \text{ K}$. An analogous scaling has been observed at similar temperatures for Cu_2IrO_3 , in

which Cu^+ ions are substituted into the Na^+ sites of Na_2IrO_3 [31]. In Figs. 1(b) and 1(c), we plot $H^{0.66}\chi(T)$ against the dimensionless variable T/H and $T^{-0.4}M(H)$ vs H/T , respectively. The $T-H$ scalings of $\chi(T)$ and $M(H)$ over nearly three orders of magnitude are consistent with the divergent power-law DOS of $N(E) \sim E^{-\alpha}$ ($\alpha = 0.34-0.4$). Our scaling exponent is found to be somewhat smaller than the reported $\alpha \approx 0.5$ [18,20–22]. The sample dependence of the nonuniversal scaling exponent implies that an amount of quenched disorders determines a specific form of the power-law DOS in the low-energy limit and thus the power-law singularities in $\chi(T)$ [30,40].

Figure 1(d) presents the T dependence of Raman spectra in (xx) polarization. Two features are discernible. Phonon modes are quite broad and a magnetic continuum increases gradually with increasing temperature for frequencies below 200 cm^{-1} , consistent with the previous work [20]. Our Raman data reveal that the random positions of H atoms strongly affect lattice vibrations involving Ir-Ir and Ir-O-Ir displacements and that the featureless continuum holds relevance for fractionalized spin excitations.

Figure 1(e) shows representative ZF- μSR spectra, which are well described by the sum of an exponentially decaying term, a Gaussian-broadened Gaussian function multiplied by a simple exponential function, and a temperature-independent background: $P_z(t) = f_1 G_{\text{GBG}}(\Delta_0, R, t) \exp(-\lambda_1 t) + f_2 \exp(-\lambda_2 t) + f_3$, where λ_1 (λ_2) is the fast (slow) muon spin relaxation rate. The Gaussian-broadened Gaussian function is given by $G_{\text{GBG}}(\Delta_0, R, t) = \frac{1}{3} + \frac{2}{3} \left(\frac{1}{1+R^2 \Delta_0^2 t^2} \right)^{3/2} \left(1 - \frac{\Delta_0^2 t^2}{1+R^2 \Delta_0^2 t^2} \right) \exp\left[-\frac{\Delta_0^2 t^2}{2(1+R^2 \Delta_0^2 t^2)}\right]$. Here, Δ_0 is the mean value of the Gaussian-broadened Gaussian distribution and R is the ratio of the distribution width W to the Gaussian mean value Δ_0 , $R = W/\Delta_0$. We observe no sign of magnetic ordering down to $T = 0.3\text{ K}$, namely, neither an oscillating signal nor a recovery to $1/3$ of the initial polarization. In Fig. 1(f), we show a semilog plot of $\lambda_i(T)$ ($i = 1, 2$) vs temperature. Both the fast relaxation $\lambda_1(T)$ and the slow relaxation $\lambda_2(T)$ are largely independent of temperature without showing enhanced magnetic correlations at low temperatures down to 0.3 K , confirming persistent spin dynamics as expected for a quantum-disordered state. Other parameters are discussed in Appendix B.

B. ^1H NMR

We now turn to the ^1H NMR results, which are the focus of the present work. Figure 2(a) presents the T dependence of ^1H NMR spectra measured for $\mu_0 H = 1\text{ T} \parallel ab$ (the honeycomb plane). On cooling down to $T = 2\text{ K}$, the ^1H NMR spectrum broadens slightly without obvious peak splitting, indicative of disordered paramagnetic behavior. As shown in Fig. 2(b), the full width at half maximum (FWHM) of the ^1H NMR spectra gradually increases with decreasing temperature down to T^* and then undergoes a rapid increase as $T \rightarrow 0\text{ K}$. We stress that the steeply increasing FWHM and the sub-Curie increase of $\chi(T)$ below T^* are commonly rooted in the growth of inhomogeneous spin fluctuations. However, the Knight shift $K(T) = (H_{\text{ref}} - H)/H \times 100\%$, bearing the intrinsic magnetic susceptibility, is nearly independent of temperature [see

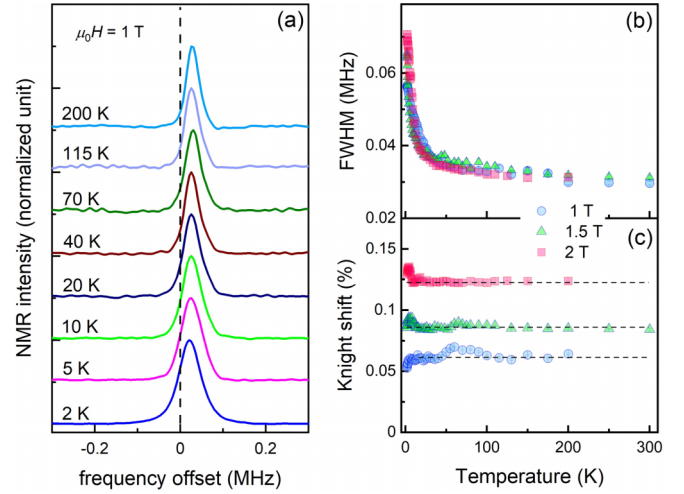


FIG. 2. (a) Temperature dependence of ^1H NMR spectra in an applied magnetic field of $\mu_0 H = 1\text{ T}$ parallel to the honeycomb ab plane. (b) Thermal evolution of the full width at half maximum of the ^1H NMR spectra. (c) Knight shift $K(T)$ vs temperature for $\mu_0 H = 1, 1.5,$ and 2 T .

Fig. 2(c)]. The lack of an apparent T dependence on $K(T)$ may be related to the fact that the ^1H NMR linewidth is larger than the thermal shift of $K(T)$ as ^1H nuclear spins experience hyperfine couplings with spatially modulated Ir^{4+} spins of distinct local spin fluctuations.

We next address the ^1H nuclear spin-lattice relaxation rate $1/T_1$, which probes the low-energy component of the \mathbf{q} -integrated spin excitation spectrum at the NMR frequency ω_0 . For comparison purposes, we first attempted to deduce $1/T_1^{\text{str}}$ from the conventional stretched fit of $M(t)$ to $1 - M(t)/M_\infty = \exp[-(t/T_1^{\text{str}})^\beta]$, where β is the stretched exponent [dashed lines in Fig. 3(a)]. Alternatively, we analyzed $M(t)$ using the ILT method based on Tikhonov regularization [solid lines in Fig. 3(a)]. We obtained the histogram $P(1/T_1)$ of the distribution of $1/T_1$ from $M(t) = \sum_i P(1/T_{1i}) [1 - \exp(-t/T_{1i})]$ with $\sum_i P(1/T_{1i}) = 1$ [15,37]. Here, $1/T_{1i}$ is the i th value of the distributed $1/T_1$. We found a better description of $M(t)$ in the ILT fit, implying that large, inhomogeneous distributions of $1/T_1$ cannot be captured within the spatially averaged value of $1/T_1^{\text{str}}$.

In Fig. 3(b), we plot the temperature dependence of $\beta(T)$. As the temperature is lowered through $T = 100\text{ K}$, $\beta \approx 0.9$ decreases to 0.4 , suggesting that a large spread of the $1/T_1$ distribution starts to develop below 100 K . Figures 3(c) and 3(d) illustrate the cascade and color contour plots of $P(1/T_1)$ in the temperature- $1/T_1$ plane, respectively. Above 100 K , $P(1/T_1)$ features a broad distribution centered around $1/T_1 \sim (0.5 - 0.05)\text{ s}^{-1}$. On cooling through 100 K , the two-peak structure in $P(1/T_1)$ becomes apparent. We recall that $\text{H}_3\text{LiIr}_2\text{O}_6$ undergoes a glassy transition of hydrogen motion at $T_g = 110\text{ K}$, involving a crossover from thermally activated hydrogen hopping to quantum tunneling [29]. As such, a switching of hydrogen dynamics is responsible for the concurrent decrease of β and the distinction of two spin dynamics (inhomogeneous magnetic states).

To shed light on the underlying spin dynamics of the two peaks, we deconvolute the $P(1/T_1)$ histogram into two

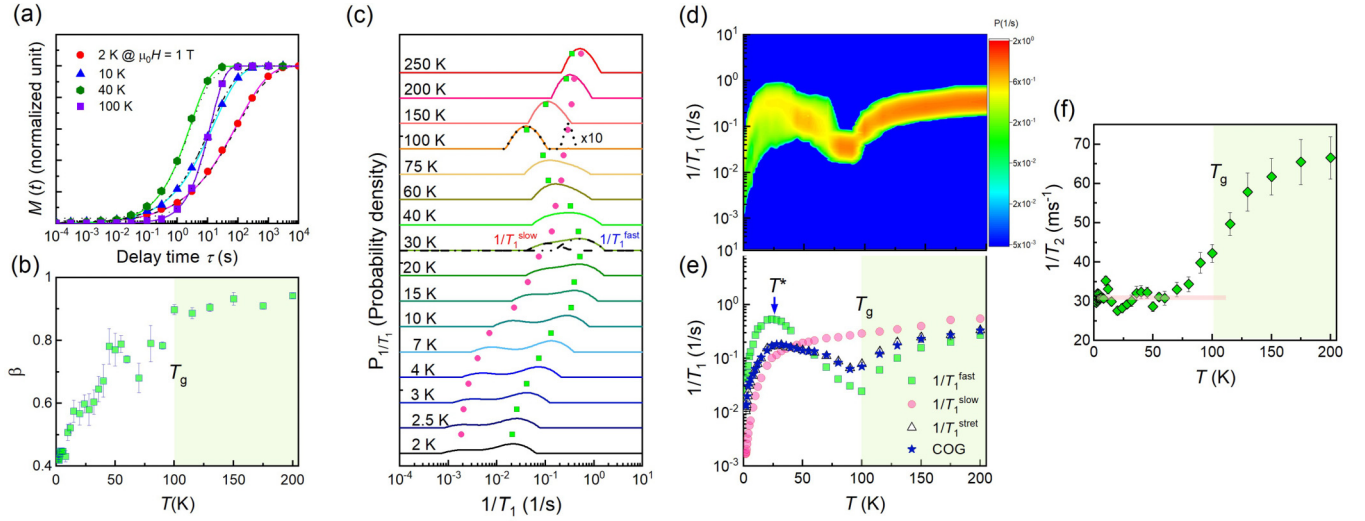


FIG. 3. (a) Stretched (dashed lines) and ILT (solid lines) fits of normalized $M(t)$ at selected temperatures. (b) Temperature dependence of the stretched exponent. (c) Distribution function $P(1/T_1)$ as a function of temperature. The symbols mark two components of $1/T_1$: $1/T_1^{\text{slow}}$ (pink circles) and $1/T_1^{\text{fast}}$ (green squares). The dash-dotted and dashed lines at 40 K and the dotted lines at 100 K are representative of two Gaussian fits. (d) The color contour plot of $P(1/T_1)$ in the temperature- $1/T_1$ plane. (e) Temperature dependence of $1/T_1^{\text{slow}}$ (pink circles), $1/T_1^{\text{fast}}$ (green squares), $1/T_1^{\text{str}}$ (open triangles), and the center of gravity (COG; stars). (f) Temperature dependence of the spin-spin relaxation rate $1/T_2$. The pink line is a guide to the eye. Pale green shadings denote a glassy transition of the hydrogen hopping at $T_g = 110$ K.

Gaussian profiles centered at $1/T_1^{\text{slow}}$ and $1/T_1^{\text{fast}}$. The dotted lines at 100 K and the dash-dotted and dashed lines at 40 K depict two representative deconvolutions used to deduce the slower and faster components of $1/T_1$. As plotted in Fig. 3(e), $1/T_1^{\text{fast}}(T)$ [green squares in Fig. 3(c)] first decreases with decreasing temperature down to 100 K and then increases as $T \rightarrow T^*$, forming a maximum at about T^* , and finally shows a power-law-like drop as $T \rightarrow 0$ K. On the other hand, the $1/T_1^{\text{slow}}(T)$ component is negligibly small for temperatures above 100 K, as seen from a 10 times magnified dotted line at $T = 100$ K in Fig. 3(c). Overall, $1/T_1^{\text{slow}}(T)$ is strongly suppressed below T^* , indicative of the formation of gapped excitations with spatially varying gaps.

We compare $1/T_1^{\text{slow}}(T)$ and $1/T_1^{\text{fast}}$ with $1/T_1^{\text{str}}(T)$ [open triangles in Fig. 3(e)]. $1/T_1^{\text{str}}(T)$ has a near-perfect overlap with the center of gravity (star symbol) of $P(1/T_1)$ and shows a nonmonotonous T dependence, featuring a dip at 80 K and a maximum around T^* . Figure 3(f) plots the thermal evolution of $1/T_2$. As the temperature is lowered from 200 K, $1/T_2$ undergoes a steplike drop and then levels off below 80 K. Noteworthy is that the spin-spin relaxation rate $1/T_2$ resembles the T dependence of $\beta(T)$ [compare Fig. 3(f) to Fig. 3(b)].

We elaborate on the Ir spin dynamics of the faster and slower relaxation components. In Fig. 4(a), we plot $1/T_1^{\text{slow}}$ vs inverse temperature on a semilogarithmic scale. It is evident that $1/T_1^{\text{slow}}$ is described by an activation form $1/T_1^{\text{slow}} \sim \exp(-\Delta/k_B T)$ with the spin gap Δ in two distinct temperature windows. Since the activation behavior is observed only over one decade, Δ should be taken as an empirical value. From fittings to the activation law, we estimate the higher- T excitation gap $\Delta_h = 30$ –38 K in the temperature range of $T = 15$ –100 K [solid lines in Fig. 4(a)] and the lower- T gap $\Delta_l = 3$ –6 K below $T = 10$ –15 K [dashed lines in Fig. 4(a)]. We note that the $\Delta_l(H)$ value is about an order of magnitude smaller than the $\Delta_h(H)$ one. The suppressed gap at low

temperatures signals the appearance of additional relaxation channels such as gapless excitations, forming random singlets [9–14]. As summarized in the inset of Fig. 4(a), $\Delta_h(H)$ (green circles) increases with increasing field from 1 T to 3 T, while $\Delta_l(H)$ (pink squares) is reduced. The opposite field dependence of $\Delta_l(H)$ and $\Delta_h(H)$ is indicative of their disparate nature. We stress that the observed gapped excitations account

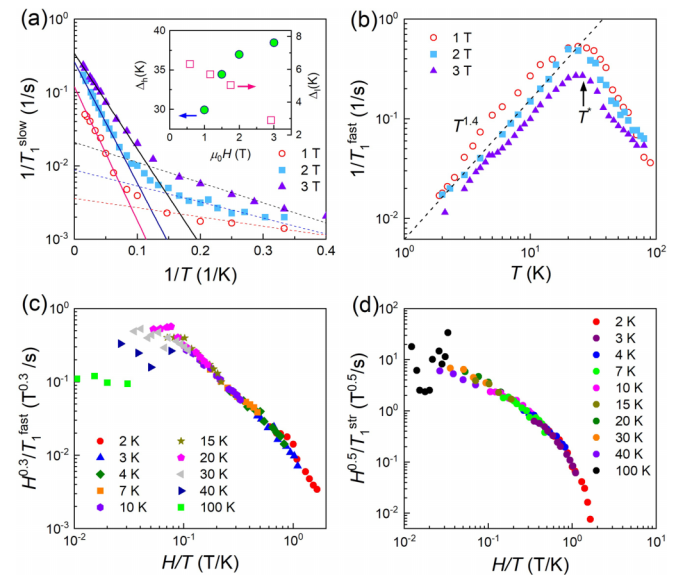


FIG. 4. (a) $1/T_1^{\text{slow}}$ as a function of inverse temperature $1/T$. The solid and dashed lines are fits to an activation behavior in two different temperature windows. The inset plots the lower- and the higher- T spin gap as a function of an applied field. (b) Log-log plot of $1/T_1^{\text{fast}}$ vs temperature at selected fields. The dashed line is a power-law fit. (c) Scaling of $H^{0.3}/T_1^{\text{fast}}$ with H/T on a double logarithmic scale. (d) Log-log scaled plot of $H^{0.5}/T_1^{\text{str}}$ versus H/T .

for only a tiny fraction of the magnetic entropy observed in the low- T specific heat [18]. Furthermore, ^{63}Cu nuclear quadrupole resonance of Cu_2IrO_3 gives evidence for gapped excitations with the gap energy of 15 meV [33]. In this vein, the gapped excitations in $\text{H}_3\text{LiIr}_2\text{O}_6$ are interpreted in view of the local modifications of Kitaev interactions by hydrogen dynamics since honeycomb layers are exchange coupled by interlayer hydrogen bonds. The random renormalization of hydrogen-disorder-induced magnetic interactions engenders a gapped phase with a gap of $(0.1\text{--}0.3)J_K$ (Kitaev interaction $J_K = 100\text{--}300$ K) [41].

Next, we discuss the disorder-induced faster $1/T_1^{\text{fast}}$ that is susceptible to the freezing of the hydrogen dynamics [29], as inferred from the kink at T_g shown by green squares in Fig. 3(e). At high temperatures above T_g , thermally activated hydrogen hopping governs spin dynamics, leading to the thermally activated behavior of $1/T_1^{\text{fast}}$ and $1/T_2$. Followed by the dip at about T_g , $1/T_1^{\text{fast}}$ forms a maximum around T^* , characteristic of short-range spin ordering, and shows the power-law dependence T^α ($\alpha \approx 1.4$) for $T < 20$ K. We further confirm the scaling behavior by plotting $H^{0.3}/T_1^{\text{fast}}$ and $H^{0.5}/T_1^{\text{str}}$ vs H/T on a double logarithmic scale in Figs. 4(c) and 4(d), respectively. The power-law scaling in spin dynamics is associated with the power-law DOS of $N(E) \sim E^{-\alpha}$ as discussed before. We note that the scaling exponent $\alpha = 0.3$ for $1/T_1^{\text{fast}}$ is somewhat smaller than $\alpha = 0.5$ for $1/T_1^{\text{str}}$. According to recent theoretical calculations of the NMR relaxation rate for the Kitaev model with disorder [40], a low- T $1/T_1$ shows a peak around $T_{\text{max}} \sim 0.05J_K$ and a power-law dependence T^α ($\alpha \leq 1$) below T_{max} for strong bond randomness or in the presence of even a small number of spin vacancies. A comparison of our NMR data to the theoretical prediction reveals that the observed superlinear $T^{1.4}$ dependence of $1/T_1^{\text{fast}}$ is stronger than the sublinear T dependence and the $(0.09\text{--}0.26)J_K$ maximum position is higher than $\sim 0.05J_K$ expected for the pure Kitaev model. The latter discrepancy may be reconciled by considering that the low- T maximum increases towards higher temperatures in extended Kitaev models [42]. The former raises the possibility that the low- T spin dynamics is dressed by random singlets and another emergent low-energy excitation.

In addition to a spin relaxation channel, quantum tunneling of hydrogen motion can contribute to $1/T_1$ in a tunneling regime (below T_g). Because quantum tunneling is independent of temperature, only a constant shift of $1/T_1$ is expected. Consequently, it does fundamentally affect our conclusion about spin dynamics.

IV. CONCLUSION

Based on the ILT analysis of the widely distributed $P(1/T_1)$ and $\chi(T)$, we draw a landscape of low-energy spin excitations in $\text{H}_3\text{LiIr}_2\text{O}_6$. We observe the emergence of magnetic inhomogeneities at about $T = 100$ K: (i) a clear separation of $P(1/T_1)$ into two peaks, (ii) a strong decrease of β ($\ll 1$), and (iii) a substantial repression of $1/T_2$. These findings demonstrate that static or dynamic hydrogen disorders, mediating interlayer interactions, modulate spin excitations. For temperatures below $T^* = 26$ K, the concurrence of the sub-Curie divergent $\chi(T) \propto T^{-0.68}$, the power-law dependent $1/T_1^{\text{fast}} \sim$

$T^{1.4}$, and the weakly activated $1/T_1^{\text{slow}} \sim \exp(-\Delta_I/k_B T)$ ($\Delta_I = 3\text{--}6$ K) provide vital clues about an intriguing quantum ground state that consists of random singlets and gapless disordered states. We recall that $s = 1/2$ kagome Heisenberg antiferromagnets possess essentially the same inhomogeneous ground state [15].

To conclude, we have employed ^1H NMR, static magnetic susceptibility, and μSR to characterize the inhomogeneous quantum ground states of $\text{H}_3\text{LiIr}_2\text{O}_6$ induced by disorders. Our ILT analysis of ^1H $1/T_1$ combined with $\chi(T)$ gives evidence that an emergent low-energy state comprises spin singlets with spatially varying small gaps and disordered quantum paramagnetic states. Our work demonstrates that the concerted influence of bond randomness and hydrogen disorder on an extended Kitaev system is far more complex than their individual effect.

ACKNOWLEDGMENTS

We acknowledge Y. Motome for valuable discussion. The work at SKKU is supported by the National Research Foundation (NRF) of Korea (Grants No. 2020R1A2C3012367 and No. 2020R1A5A1016518).

APPENDIX A: XRD AND RAMAN SPECTRA

Figure 5(a) shows XRD patterns at room temperature for $\alpha\text{-Li}_2\text{IrO}_3$ and $\text{H}_3\text{LiIr}_2\text{O}_6$. The XRD patterns of two iridate oxides exhibit three diffraction peaks indexed with (001), (002), and (003) in the $C2/m$ monoclinic setting. The 2θ of (001) peak is shifted up from 18.44° for $\alpha\text{-Li}_2\text{IrO}_3$ to 19.24° for $\text{H}_3\text{LiIr}_2\text{O}_6$, corresponding to interlayer distances 5.12 and 4.94 Å, respectively. This decrease in the interlayer distance is due to the replacement of Li^+ ions with H^+ ions between layers.

Figure 5(b) compares the $T = 300$ Raman spectra between $\alpha\text{-Li}_2\text{IrO}_3$ and $\text{H}_3\text{LiIr}_2\text{O}_6$ in (xx) polarization. The Raman result indicates that H^+ ions are perfectly absorbed in the $\alpha\text{-Li}_2\text{IrO}_3$ sample. In Fig. 5(c), we show the (xx) and (xy) polarized Raman spectra. A previous Raman study of $\text{H}_3\text{LiIr}_2\text{O}_6$ reported a total of seven phonon modes $2A_g + 1B_g + 4(A_g + B_g)$ [20]. We observe five phonon modes: two A_g modes at 347 and 624 cm^{-1} and three $(A_g + B_g)$ modes at 235, 473, and 540 cm^{-1} . The other two peaks were not visible in our Raman spectrum due to a weak scattering intensity. Compared to Pei *et al.* [20], the phonon frequencies of our sample shift to lower energies by 6–19 cm^{-1} . Further, we note that our sample shows less pronounced quasielastic scattering at high temperatures than Shanghai's sample.

APPENDIX B: μSR

Figure 6 shows the temperature dependence of the fitting parameters obtained from the ZF- μSR results in the temperature range of $T = 0.3\text{--}10$ K. The fast relaxation rate λ_1 increases slightly with decreasing temperature and nearly levels off below 3 K, while the slow relaxation rate λ_2 displays a nearly temperature-independent behavior. This suggests a quantum-disordered ground state with persistent spin dynamics. In addition, the internal field distribution Δ_0 , the ratio R ,

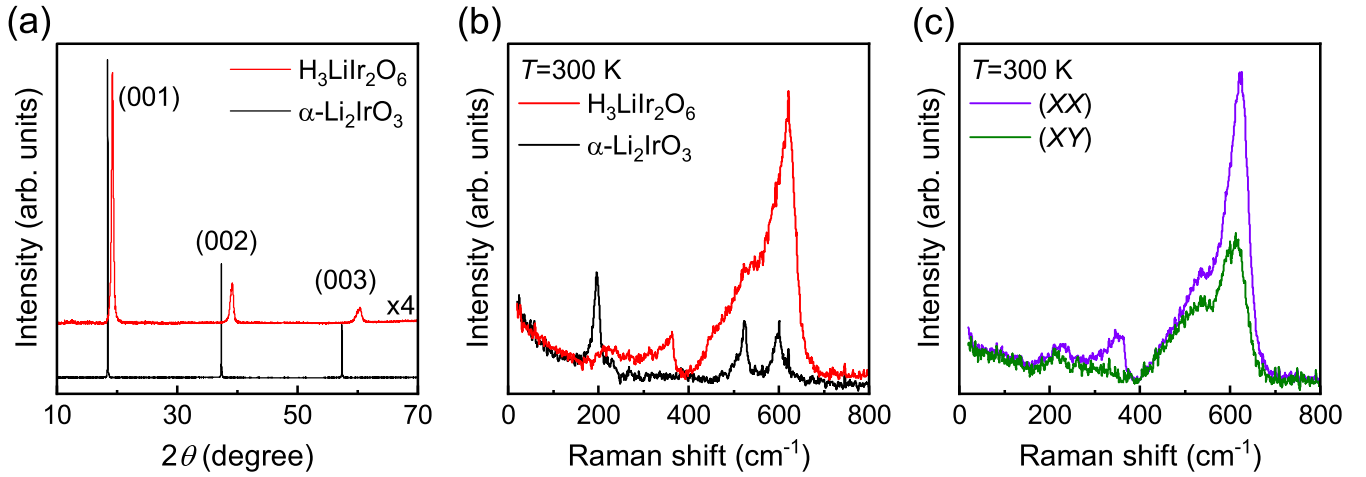


FIG. 5. (a) X-ray diffraction patterns of $\alpha\text{-Li}_2\text{IrO}_3$ and $\text{H}_3\text{LiIr}_2\text{O}_6$ at room temperature. Peaks are indexed with Miller (00l) indices. (b) Raman spectra of $\alpha\text{-Li}_2\text{IrO}_3$ and $\text{H}_3\text{LiIr}_2\text{O}_6$ at room temperature. (c) Polarized Raman spectra of $\text{H}_3\text{LiIr}_2\text{O}_6$ at room temperature in (xx) and (xy) polarizations.

and the fast-relaxing fraction f_1 are also temperature independent. The average values of the parameters are evaluated to be $\Delta_0^{\text{avg}} = 11.76$ MHz, $R = 0.39$, and $f_1^{\text{avg}} = 0.372$, respectively. It should be noted that the Gaussian-broadened Gaussian function is appropriate to describe the muon spin depolarization driven by disordered magnetism with short-range correlations.

In order to separate the static and dynamic fractions, we carried out LF- μ SR experiments at $T = 0.3$ K. As depicted in Fig. 7, with increasing the longitudinal field H_{LF} , the muon spin polarization begins to recover and is fully saturated at $H_{\text{LF}} = 4500$ G. The obtained LF- μ SR spectra are well

described by the sum of dynamic Gaussian Kubo-Toyabe, simple exponential, and constant background: $P_z(t) = f_1 G_{\text{DGKT}}(\Delta, H_{\text{LF}}, \nu, t) \exp(-\lambda_1 t) + f_2 \exp(-\lambda_2 t) + f_3$. Here, $G_{\text{DGKT}}(\Delta, H_{\text{LF}}, \nu, t)$ is the dynamic Gaussian Kubo-Toyabe function with the applied field H_{LF} and the fluctuation rate ν . The μ SR asymmetry was normalized by the fitted theoretical value after subtracting the temperature-independent background f_3 . The fittings to the LF- μ SR data provide the field distribution $\Delta = 11.08(3)$ MHz and the nearly zero hopping term $\nu = 4.4$ kHz. The static and dynamic fractions are estimated to be 72.4% and 27.6%, respectively. In contrast to the previous μ SR results [19], however, we could not identify the time-field scaling $P_z(t) = P(t/H^\gamma)$ of the LF- μ SR spectra.

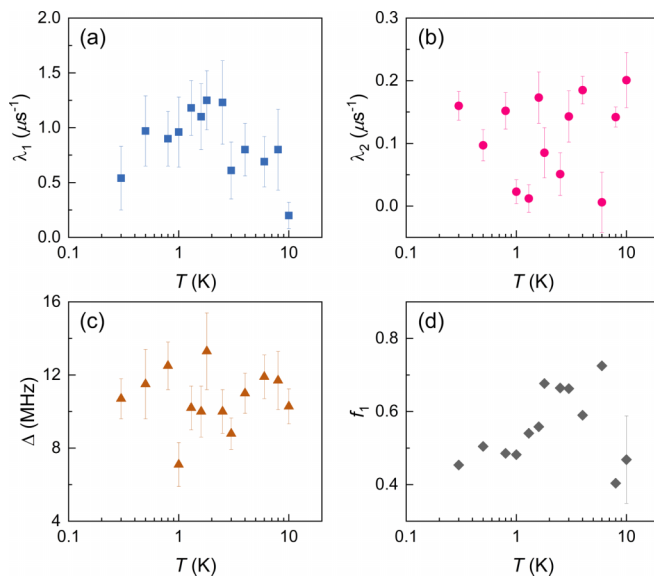


FIG. 6. (a) Temperature dependence of the ZF- μ SR fitting parameters. Fast- and slow-muon spin relaxation rates λ_1 and λ_2 vs temperature in a semilog scale. (b) Temperature dependence of the mean value of the Gaussian-broadened Gaussian distribution Δ_0 . (c) Ratio of the distribution width to the distribution mean value. (d) Thermal evolution of the fast-relaxing fraction f_1 .

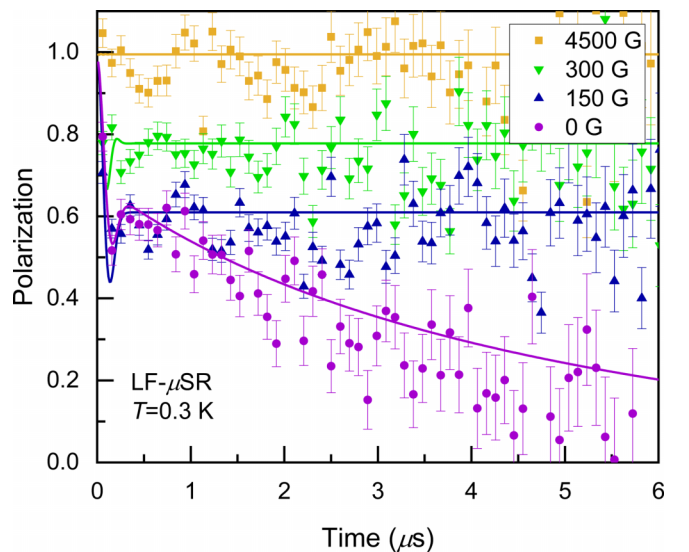


FIG. 7. LF dependence of μ SR spectra at $T = 0.3$ K in representative fields. The solid curves indicate the fittings to the data as described in the text. The internal field/frequency distribution is evaluated to be $\Delta = 11.08(3)$ MHz.

- [1] A. Kitaev, Anyons in an exactly solved model and beyond, *Ann. Phys. (NY)* **321**, 2 (2006).
- [2] G. Jackeli and G. Khaliullin, Mott Insulators in the Strong Spin-Orbit Coupling Limit: From Heisenberg to a Quantum Compass and Kitaev Models, *Phys. Rev. Lett.* **102**, 017205 (2009).
- [3] Y. Singh and P. Gegenwart, Antiferromagnetic Mott insulating state in single crystals of the honeycomb lattice material Na_2IrO_3 , *Phys. Rev. B* **82**, 064412 (2010).
- [4] Y. Singh, S. Manni, J. Reuther, T. Berlijn, R. Thomale, W. Ku, S. Trebst, and P. Gegenwart, Relevance of the Heisenberg-Kitaev Model for the Honeycomb Lattice Iridates A_2IrO_3 , *Phys. Rev. Lett.* **108**, 127203 (2012).
- [5] K. W. Plumb, J. P. Clancy, L. J. Sandilands, V. V. Shankar, Y. F. Hu, K. S. Burch, H.-Y. Kee, and Y.-J. Kim, $\alpha - \text{RuCl}_3$: A spin-orbit assisted Mott insulator on a honeycomb lattice, *Phys. Rev. B* **90**, 041112(R) (2014).
- [6] S.-H. Do, S.-Y. Kwon, D. T. Park, J. Yoshitake, J. Voneshen, Y. Motome, Y. S. Kwon, D. T. Adroja, D. J. Voneshen, K. Kim, T.-H. Jang, J.-H. Park, K.-Y. Choi, and S. Ji, Majorana fermions in the Kitaev quantum spin system $\alpha - \text{RuCl}_3$, *Nat. Phys.* **13**, 1079 (2017).
- [7] H. Takagi, T. Kakayama, G. Jackeli, G. Khaliullin, and S. E. Nagler, Concept and realization of Kitaev quantum spin liquids, *Nat. Rev. Phys.* **1**, 264 (2019).
- [8] S. Trebst and C. Hickey, Kitaev materials, *Phys. Rep.* **950**, 1 (2022).
- [9] K. Watanabe, H. Kawamura, H. Nakano, and T. Sakai, Quantum spin-liquid behavior in the spin-1/2 random Heisenberg antiferromagnet on the triangular lattice, *J. Phys. Soc. Jpn.* **83**, 034714 (2014).
- [10] L. Savary and L. Balents, Disorder-Induced Quantum Spin Liquid in Spin Ice Pyrochlores, *Phys. Rev. Lett.* **118**, 087203 (2017).
- [11] I. Kimchi, A. Nahum, and T. Senthil, Valence Bonds in Random Quantum Magnets: Theory and Application to YbMgGaO_4 , *Phys. Rev. X* **8**, 031028 (2018).
- [12] L. Liu, H. Shao, Y.-C. Lin, W. Guo, and A. W. Sandvik, Random-Singlet Phase in Disordered Two-Dimensional Quantum Magnets, *Phys. Rev. X* **8**, 041040 (2018).
- [13] H. Kawamura and K. Uematsu, Nature of the randomness-induced quantum spin liquids in two dimensions, *J. Phys.: Condens. Matter* **31**, 504003 (2019).
- [14] S. Sanyal, K. Damle, J. T. Chalker, and R. Moessner, Emergent Moments and Random Singlet Physics in a Majorana Spin Liquid, *Phys. Rev. Lett.* **127**, 127201 (2021).
- [15] J. Wang, W. Yuan, P. M. Singer, R. W. Smaha, W. He, J. Wen, Y. S. Lee, and T. Imai, Emergence of spin singlets with inhomogeneous gaps in the kagome lattice Heisenberg antiferromagnets Zn-barlowite and herbertsmithite , *Nat. Phys.* **17**, 1109 (2021).
- [16] T. Shiroka, F. Eggenschwiler, H.-R. Ott, and J. Mesot, From order to randomness: Onset and evolution of the random-singlet state in bond-disordered $\text{BaCu}_2(\text{Si}_{1-x}\text{Ge}_x)_2\text{O}_7$ spin-chain compounds, *Phys. Rev. B* **99**, 035116 (2019).
- [17] S. Bette, T. Takayama, K. Kitagawa, R. Takano, H. Takagi, and R. E. Dinnebier, Solution of the heavily stacking faulted crystal structure of the honeycomb iridate $\text{H}_3\text{LiIr}_2\text{O}_6$, *Dalton Trans.* **46**, 15216 (2017).
- [18] K. Kitagawa, T. Takayama, Y. Matsumoto, A. Kato, R. Takano, Y. Kishimoto, S. Bette, R. Dinnebier, G. Jackeli, and H. Takagi, A spin-orbital-entangled quantum liquid on a honeycomb lattice, *Nature (London)* **554**, 341 (2018).
- [19] Y.-X. Yang, L.-L. Huang, Z.-H. Zhu, C.-S. Chen, Q. Wu, Z.-F. Ding, C. Tan, P. K. Biswas, A. D. Hillier, Y.-G. Shi, D.-P. Yu, C. Liu, L. Wang, F. Ye, J.-W. Mei, and L. Shu, Muon Spin Relaxation Study of Spin Dynamics in Quantum Spin Liquid Candidate $\text{H}_3\text{LiIr}_2\text{O}_6$, [arXiv:2201.12978](https://arxiv.org/abs/2201.12978).
- [20] S. Pei, L.-L. Huang, G. Li, X. Chen, B. Xi, X. W. Wang, Y. Shi, D. Yu, C. Liu, L. Wang, F. Ye, M. Huang, and J.-W. Mei, Magnetic Raman continuum in single-crystalline $\text{H}_3\text{LiIr}_2\text{O}_6$, *Phys. Rev. B* **101**, 201101(R) (2020).
- [21] J. Knolle, R. Moessner, and N. B. Perkins, Bond-Disordered Spin Liquid and the Honeycomb Iridate $\text{H}_3\text{LiIr}_2\text{O}_6$: Abundant Low-Energy Density of States from Random Majorana Hopping, *Phys. Rev. Lett.* **122**, 047202 (2019).
- [22] W.-H. Kao, J. Knolle, G. B. Halasz, R. Moessner, and N. B. Perkins, Vacancy-Induced Low-Energy Density of States in the Kitaev Spin Liquid, *Phys. Rev. X* **11**, 011034 (2021).
- [23] R. Yadav, R. Ray, M. S. Eldeeb, S. Nishimoto, L. Hozoi, and J. van den Brink, Strong Effect of Hydrogen Order on Magnetic Kitaev Interactions in $\text{H}_3\text{LiIr}_2\text{O}_6$, *Phys. Rev. Lett.* **121**, 197203 (2018).
- [24] Y. Li, S. M. Winter, and R. Valentí, Role of Hydrogen in the Spin-Orbital-Entangled Quantum Liquid Candidate $\text{H}_3\text{LiIr}_2\text{O}_6$, *Phys. Rev. Lett.* **121**, 247202 (2018).
- [25] K. Slagle, W. Choi, L. E. Chern, and Y. B. Kim, Theory of a quantum spin liquid in the hydrogen-intercalated honeycomb iridate $\text{H}_3\text{LiIr}_2\text{O}_6$, *Phys. Rev. B* **97**, 115159 (2018).
- [26] R. Yadav, M. S. Eldeeb, R. Ray, S. Aswartham, M. I. Sturza, S. Nishimoto, J. van den Brink, and L. Hozoi, Engineering Kitaev exchange in stacked iridate layers: Impact of interlayer species on in-plane magnetism, *Chem. Sci.* **10**, 1866 (2019).
- [27] S. Wang, L. Zhang, and F. Wang, Possible quantum paraelectric state in Kitaev spin liquid candidate $\text{H}_3\text{LiIr}_2\text{O}_6$, *Sci. China Phys. Mech. Astron.* **63**, 117411 (2020).
- [28] F. Zschecke and M. Vojta, *Phys. Rev. B* **92**, 014403 (2015).
- [29] K. Geirhos, P. Lunkenheimer, M. Blankenhorn, R. Claus, Y. Matsumoto, K. Kitagawa, T. Takayama, H. Takagi, I. Kézsmárki, and A. Loidl, Quantum paraelectricity in the Kitaev quantum spin liquid candidates $\text{H}_3\text{LiIr}_2\text{O}_6$ and $\text{D}_3\text{LiIr}_2\text{O}_6$, *Phys. Rev. B* **101**, 184410 (2020).
- [30] V. Dantas and E. C. Andrade, Disorder, Low-Energy Excitations, and Topology in the Kitaev Spin Liquid, *Phys. Rev. Lett.* **129**, 037204 (2022).
- [31] Y. S. Choi, C. H. Lee, S. Lee, S. Yoon, W.-J. Lee, J. Park, A. Ali, Y. Singh, J.-C. Orain, G. Kim, J.-S. Rhyee, W.-T. Chen, F. Chou, and K.-Y. Choi, Exotic Low-Energy Excitations Emergent in the Random Kitaev Magnet, *Phys. Rev. Lett.* **122**, 167202 (2019).
- [32] F. Bahrami, W. Lafargue-Dit-Hauret, O. I. Lebedev, R. Movshovich, H.-Y. Yang, D. Broido, X. Rocquefelte, and F. Tafti, Thermodynamic Evidence of Proximity to a Kitaev Spin Liquid in $\text{Ag}_3\text{LiIr}_2\text{O}_6$, *Phys. Rev. Lett.* **123**, 237203 (2019).
- [33] S. K. Takahashi, J. Wang, A. Arsenault, T. Imai, M. Abramchuk, F. Tafti, and P. M. Singer, Spin Excitations of a Proximate Kitaev Quantum Spin Liquid Realized in Cu_2IrO_3 , *Phys. Rev. X* **9**, 031047 (2019).
- [34] S.-H. Do, C. H. Lee, T. Kihara, Y. S. Choi, S. Yoon, K. Kim, H. Cheong, W.-T. Chen, F. Chou, H. Nojiri, and K.-Y.

- Choi, Randomly Hopping Majorana Fermions in the Diluted Kitaev System $\alpha - \text{Ru}_{0.8}\text{Ir}_{0.2}\text{Cl}_3$, *Phys. Rev. Lett.* **124**, 047204 (2020).
- [35] S.-H. Baek, H. W. Yeo, S.-H. Do, K.-Y. Choi, L. Janssen, M. Vojta, and B. Büchner, Observation of a random singlet state in a diluted Kitaev honeycomb material, *Phys. Rev. B* **102**, 094407 (2020).
- [36] J. Wang, W. Yuan, T. Imai, P. M. Singer, F. Bahrami, and F. Tafti, NMR investigation on the honeycomb iridate $\text{Ag}_3\text{LiIr}_2\text{O}_6$, *Phys. Rev. B* **103**, 214405 (2021).
- [37] P. M. Singer, A. Arsenault, T. Imai, and M. Fujita, ^{139}La NMR investigation of the interplay between lattice, charge, and spin dynamics in the charge-ordered high-Tc cuprate $\text{La}_{1.875}\text{Ba}_{0.125}\text{CuO}_4$, *Phys. Rev. B* **101**, 174508 (2020).
- [38] F. Freund, S. C. Williams, R. D. Johnson, R. Coldea, P. Gegenwart, and A. Jesche, Single crystal growth from separated educts and its application to lithium transition-metal oxides, *Sci. Rep.* **6**, 35362 (2016).
- [39] A. Suter and B. M. Wojek, Musrfit: A Free Platform-Independent Framework for μSR Data Analysis, *Phys. Proc.* **30**, 69 (2012).
- [40] J. Nasu and Y. Motome, Spin dynamics in the Kitaev model with disorder: Quantum Monte Carlo study of dynamical spin structure factor, magnetic susceptibility, and NMR relaxation rate, *Phys. Rev. B* **104**, 035116 (2021).
- [41] J. Knolle, D. L. Kovrizhin, J. T. Chalker, and R. Moessner, Dynamics of fractionalization in quantum spin liquids, *Phys. Rev. B* **92**, 115127 (2015).
- [42] Y. Yamaji, T. Suzuki, T. Yamada, S. Suga, N. Kawashima, and M. Imada, Clues and criteria for designing a Kitaev spin liquid revealed by thermal and spin excitations of the honeycomb iridate Na_2IrO_3 , *Phys. Rev. B* **93**, 174425 (2016).